Article

Epidermal Growth Factor Receptor-Targeted Delivery of a Singlet Oxygen Sensitizer with Thermal Controlled Release for Efficient Anticancer Therapy

Juanjuan Chen, Dongyao Li, Beibei Huo, Fengling Zhang, Xuan Zhao, Gankun Yuan, Dan Chen, Meiru Song, and Jinping Xue

Mol. Pharmaceutics, **Just Accepted Manuscript** • DOI: 10.1021/acs.molpharmaceut.9b00670 • Publication Date (Web): 25 Jun 2019

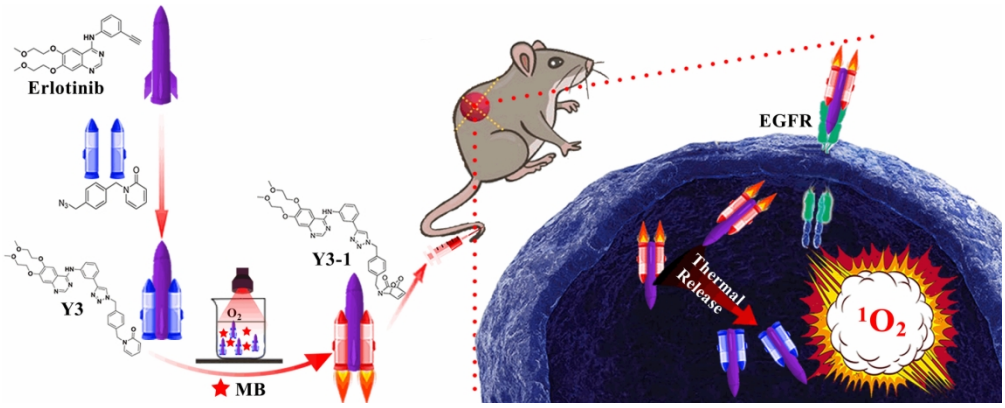

Y3-1, which contains a small molecular-targeted agent and a singlet oxygen thermal-controlled releasing moiety, exhibits excellent erlotinib-based tumor targeting delivery and enhanced PDT- mimetic anticancer activities.

82x32mm (600 x 600 DPI)

Epidermal Growth Factor Receptor-Targeted Delivery of a Singlet Oxygen Sensitizer with Thermal Controlled Release for Efficient Anticancer Therapy

Juanjuan Chen,[†,⊥] Dongyao Li,[†,⊥] Beibei Huo,[†] Fengling Zhang,[‡] Xuan Zhao,[†] Gankun Yuan,[†] Dan Chen,[†] Meiru Song,[†] and Jinping Xue[*,†]*

[†]National and Local Joint Biomedical Engineering Research Center on Photodynamic Technologies, College of Chemistry, Fuzhou University, Fuzhou 350116, Fujian, China.

[‡]College of Pharmaceutical Science, Zhejiang Chinese Medical University, Hangzhou 310053, Zhejiang, China.

KEYWORDS: targeted delivery, erlotinib, singlet oxygen release, 2-pyridone, anticancer therapy

ABSTRACT. Photodynamic therapy (PDT) utilizing light-induced singlet oxygen has achieved attractive results in anticancer fields; however, its development is hindered by limited light penetration depth, skin phototoxicity, tumor hypoxia and PDT-induced hypoxia. Inspired by our previous research work and the limitations of PDT, we introduce a small-molecule targeted drug erlotinib into the singlet oxygen chemical source endoperoxide to achieve an EGFR-targeted

PDT-mimetic sensitizer (**Y3-1**) for anticancer therapy. We demonstrated that the erlotinib-based precise delivery of the singlet oxygen chemical source (*in vitro* photosensitization) to EFGR-overexpressing tumor cells and tissues. Moreover, the anticancer assays validated that the enhanced anticancer efficacy (*in vitro* and *in vivo*) of **Y3-1** was due to reversible singlet oxygen thermal release. This study is expected to provide a smart strategy to break through the current roadblock in targeted PDT and achieve a more efficient anticancer therapy model.

INTRODUCTION.

Photodynamic therapy (PDT) has been considered as a specific and controllable therapeutic modality for cancer.[1-4] During PDT in cancer, the synergistic action of photosensitizers (PSs), light and oxygen in the tumor region can generate highly reactive singlet oxygen ($^1O_2$), which results in cell apoptosis or necrosis, shut down the tumor microvasculature and induce the anticancer immune response.[2,5-6] PDT has tremendous therapeutic potential because of its advantages such as minimal invasiveness, negligible drug resistance, and quick recovery.[1-5,7] However, there are still some drawbacks that must be overcome to realize the full promise of PDT in anticancer treatment.First, the light, which is needed for the generation of singlet oxygen, cannot penetrate tissues to more than a few millimeters.[8-10]In addition, photosensitizers accumulation in skin during PDT will lead to skin phototoxicity upon exposure to light.[11-12] Second, tumor hypoxia and PDT-induced hypoxia seriously hinder effective singlet oxygen generation, which makes PDT a self-limiting method.[13-15]Finally, the PDT dosimetry problem, which relates to the photosensitizer, light and oxygen, still limits the clinical application of PDT.[7,16-17] These problems are not only due to the lack of ideal photosensitizers or smart delivery/activation strategies, but also lie at the core of the PDT paradigm.

Inspired by the fact that highly reactive singlet oxygen is the critical and ultimate cytotoxic factor during effective PDT, we propose a smart strategy to circumvent all of these issues. Singlet oxygen can be produced by *in vitro* photosensitization with sufficient oxygen concentration and then stored by a chemical method; finally, the trapped singlet oxygen can be precisely delivered into the tumor region and reversibly release singlet oxygen for anticancer therapy. This smart strategy is supposed to resolve the problems of oxygen and skin phototoxicity in PDT. Moreover, this approach is free of the *in vivo* use of complicated laser instruments and has potential application in the treatment of deep-seated tumors.

The ideal chemical sources of singlet oxygen should have high $^1O_2$ yields and no side reactions in the cell. The endoperoxides of 2-pyridone and its derivatives have been demonstrated to be excellent chemical sources with clean cycloreversion reactions with very high $^1O_2$ yields.[18-21] They can decompose to release $^1O_2$ under thermal conditions and result in cancer cell death.[21-22]In addition, 2-pyridone and its derivatives can trap singlet oxygen to form endoperoxides by photosensitization.[19-22] In fact, there are some reports about photosensitizer endoperoxide derivatives[22-25] and controlled release of $^1O_2$ by gold nanorod.[26] However, these former sensitizers still depend on *in vivo* light and oxygen concentration in tumor region because of self-photosensitization, and the latter requires 808 nm laser irradiation. More importantly, they all suffer from poor cancer targeting which may result in damage to normal tissues and organs. Thus, it is desirable to develop cancer-targeted delivery of singlet oxygen chemical sources.

Erlotinib (Tarceva), a small-molecule targeted anticancer drug, can target the ATP binding domain of tyrosine kinase in epidermal growth factor receptor (EGFR) overexpressing tumors and exhibits specific affinity to tumor cells.[27-30] Our previous research work showed that it can successfully deliver phthalocyanine photosensitizers to EGFR-overexpressing tumors with high

selectivity.[31-35] Based on the above consideration, we introduced erlotinib into a 2-pyridone endoperoxide for precise delivery of the $^1O_2$ provider (generated through an *in vitro* photodynamic reaction) for targeted anticancer therapy. A novel compound (**Y3-1**) was designed and prepared through a click chemistry reaction. **Y3-1** shows the temperature-sensitive release ability of $^1O_2$ with a $t_{1/2}$ value of 13 h at 37 °C, high specific affinity and anticancer activities to EGFR-overexpressing cancer cells and tumor tissue. This work may not only hope to break through the reliance of PDT on light, oxygen and PS, but also improve the efficacy of small-molecule targeted anticancer drugs. More importantly,an accuratedosimetric description of singlet oxygen-based anticancer therapy may become feasible by this strategy, because of the quantitative supply of $^1O_2$ in this unimolecular system. To the best of our knowledge, this is the first report of the precise application of EGFR-targeted anticancer drug to precisely deliver the $^1O_2$ chemical sources to the tumor region.

MATERIALS AND METHODS

Chemicals and Instruments. All solvents and chemicals were purchased from Sinopharm Chemical Reagent Co., Ltd and were subjected to treatments of deoxygenation and dehydration. Mito-Tracker Green, Lyso-Track red, DAPI (1,3-diphenylisobenzofuran), ROS (reactive oxygen species;) detection kits and BCA protein assay kits were purchased from Beyotime Biotechnology Co., Ltd. MTT (3-[4,5-dimethylthiazol-2-yl]-2,5-diphenyltetrazolium bromide) were purchased from Sigma Chemical Corp. Roswell Park Memorial Institute 1640 (RPMI-1640) medium and trypsin-EDTA solution were purchased from Gibco Life Technologies. Annexin V-FITC/PI apoptosis detection kits were purchased from BD Company. All cell lines were provided by Institute of Life Sciences, Chinese Academy of Sciences. ^{1}H NMR and ^{13}C NMR spectra were recorded on nuclear magnetic resonance with models of AVANCE III (400 or 500

MHz). Data of HRMS were detected by LC-QTOF-MS (G6520B). Purity of all final compounds was 95% or higher. Detecting the ability of **Y3-1** to release $^1O_2$ using a Lambda 365-UV-Visible absorption spectrometer. Other instruments include a microplate reader (PerkinElmer Corporation), BD AccuriTM C6 Flow cytometer (Becton Dickinson), FV-1000 laser confocal scanning microscope (Olympus Corporation). The *in vivo* fluorescence imaging was performed by i*n vivo* fluorescence molecular tomography (FMT) using the FMTTM 2500 system (PerkinElmer Corporation).

Synthesis. *Compound **Y1***. Alpha,alpha'-Dibromo-p-xylene (1.218 g, 4.614 mmol) and NaN_3 (0.3019 g, 4.644 mmol) were dissolved in DMF(10 mL) and stirred at room temperature overnight. The crude products were purified by silica gel column chromatography (PE: CH_2Cl_2 = 20:1) to give compound **Y1** (0.3985 g, 38.2%) as a white crystal. ^{1}H NMR (400 MHz, $CDCl_3$): δ 7.44 (d, J = 8.0 Hz, 2H), 7.33 (d, J = 8.0 Hz, 2H), 4.52 (s, 2H), 4.37 (s, 2H). ^{13}C NMR (126 MHz, DMSO-d_6): δ 138.38, 136.24, 130.07, 129.20, 129.14, 53.70, 34.47.

*Compound **Y2***. Compound **Y1** (0.3985 g, 1.762 mmol) was dissolved in DMF (10 mL) and 2-hydroxypyridine (0.2534 g, 2.665 mmol) was added, and then K_2CO_3 (0.2920 g, 2.113 mmol) 18-Crown and KI were added as catalyst. The mixture was stirred at room temperature overnight. The crude products were purified by silica gel column chromatography (CH_2Cl_2:CH_3OH = 100:1); Compound **Y2** was obtained as a colorless liquid (0.3564 g, 84.2%). ^{1}H NMR (400 MHz, DMSO-d_6): δ 7.80 (d, J = 6.4 Hz, 1H), 7.47 – 7.39 (m, 1H), 7.33 (q, J = 8.1 Hz, 4H), 6.43 (d, J = 9.1 Hz, 1H), 6.25 (t, J = 6.7 Hz, 1H), 5.11 (s, 2H), 4.43 (s, 2H). ^{13}C NMR (126 MHz, DMSO-d_6): δ 161.88, 140.56, 139.58, 137.84, 135.35, 129.08, 128.44, 120.37, 106.02, 53.74, 51.33. HRMS (ESI): m/z 240.1011, calcd for $C_{13}H_{12}N_4O$ $[M+H]^+$: 241.1084, found for $[M+H]^+$: 241.1084, Δ = 0.41 ppm.

*Compound **Y2-1**.* Compound **Y2** (0.5477 g, 2.2779 mmol) and MB (0.0544 g, 0.1700 mmol) were dissolved in $CDCl_3$ (10 mL) and illuminated by 670 nm laser (1 W) in presence of oxygen at -20 °C for 4 h with stirring. When the reaction was completed, the crude product was purified by silica gel column chromatography by the frozen CH_2Cl_2 (0 °C) to give compound **Y2-1** (0.1868 g, 30.1%) as a dark yellow liquid. ^{1}H NMR (500 MHz, $CDCl_3$): δ 7.30 (d, J = 7.8 Hz, 2H), 7.23 (d, J = 7.8 Hz, 2H), 6.73 (tt, J = 9.1, 6.4 Hz, 2H), 5.55 (dd, J = 5.1, 2.1 Hz, 1H), 5.06 (dt, J = 5.7, 1.8 Hz, 1H), 4.84 – 4.77 (m, 1H), 4.45 (d, J = 15.4 Hz, 1H), 4.33 (s, 2H). ^{13}C NMR (126 MHz, $CDCl_3$): δ 168.29, 135.53, 135.34, 134.39, 128.87, 128.82, 128.37, 83.47, 78.08, 54.33, 53.58, 46.72. HRMS (ESI): m/z 272.2640, calcd for $C_{13}H_{12}N_4NaO_3$ $[M+Na]^+$: 295.0802, found for $[M+Na]^+$: 295.0811, Δ = 3.05 ppm.

*Compound **Y3**.* Compound **Y2** (0.3568 g, 1.483 mmol) and erlotinib (0.8754 g, 2.225 mmol) were dissolved in mixture solvent (THF/H_2O/tBu-OH, 8/4/6 mL) with $CuSO_4 \cdot 5H_2O$ and sodium ascorbate was added as a catalyst. The mixture was stirred at room temperature overnight. The crude product was purified by silica gel column chromatography (CH_2Cl_2:CH_3OH from 100:1 to 20:1) to give compound **Y3** (0.8368 g, 89.0%) as a light-yellow solid. ^{1}H NMR (400 MHz, DMSO-d_6): δ 9.58 (s, 1H), 8.63 (s, 1H), 8.48 (s, 1H), 8.23 (s, 1H), 7.96 – 7.86 (m, 2H), 7.77 (d, J = 6.7 Hz, 1H), 7.54 (d, J = 7.7 Hz, 1H), 7.47 – 7.38 (m, 2H), 7.32 (q, J = 8.1 Hz, 4H), 7.23 (s, 1H), 6.40 (d, J = 9.1 Hz, 1H), 6.22 (t, J = 6.6 Hz, 1H), 5.63 (s, 2H), 5.08 (s, 2H), 4.35 – 4.26 (m, 4H), 3.82 – 3.72 (m, 4H), 3.38 (s, 3H), 3.36 (s, 3H). ^{13}C NMR (101 MHz, DMSO-d_6): δ 161.86, 154.05, 148.57, 147.14, 140.58, 140.51, 139.56, 137.93, 135.72, 131.39, 129.46, 128.69, 128.60, 122.27, 122.05, 120.79, 120.35, 119.24, 106.03, 103.73, 70.62, 70.54, 68.84, 68.51, 58.88, 58.82, 53.22, 51.28. HRMS (ESI): m/z 633.2700, calcd for $C_{35}H_{35}N_7O_5$ $[M+H]^+$: 634.2772, found for $[M+H]^+$: 634.2799, Δ = 1.10 ppm.

*Compound **Y3-1***. Compound **Y2-1** (0.2000 g, 0.7346 mmol) and erlotinib (0.2981g, 0.7577 mmol) were dissolved in mixture solvent ($CHCl_3$/H_2O/tBu-OH, 8/4/6/2 mL) with $CuSO_4.5H_2O$ and sodium ascorbate was added as a catalyst. The mixture was stirred at 3 °C overnight. When the reaction was completed, the crude product was purified by silica gel column chromatography 3 times by the frozen solvent (CH_2Cl_2:CH_3OH from 100:1 to 20:1, 0 °C). After cold vacuum distillation (0 °C), compound **Y3-1** (0.0467 g, 8.43%) was obtained as the white solid. ^{1}H NMR (500 MHz, DMSO-d_6): δ 9.46 (s, 1H), 8.54 (d, J = 2.5 Hz, 1H), 8.23 (d, J = 1.9 Hz, 1H), 7.95 (d, J = 1.8 Hz, 1H), 7.91 (d, J = 6.5 Hz, 2H), 7.62 (d, J = 1.8 Hz, 1H), 7.53 (dt, J = 7.7, 1.3 Hz, 1H), 7.42 (t, J = 7.9 Hz, 1H), 7.30 (s, 1H), 7.28 (s, 1H), 7.21 (d, J = 1.7 Hz, 2H), 7.19 (s, 1H), 5.88 (d, J = 6.5 Hz, 1H), 5.58 (s, 2H), 4.52 (s, 1H), 4.35 (dd, J = 5.7, 4.2 Hz, 2H), 4.31 – 4.27 (m, 2H), 4.10 (dd, J = 6.4, 1.7 Hz, 1H), 3.88 – 3.84 (m, 4H), 3.71 (dd, J = 4.1, 1.7 Hz, 1H), 3.62 (d, J = 4.1 Hz, 1H), 3.48 (d, J = 4.1 Hz, 6H). HRMS (ESI): m/z 665.2598, calcd for $C_{37}H_{40}N_7O_9$ $[M+CH_3COOH]^+$: 726.2882 , found for $[M+CH_3COOH]^+$: 726.2895 , Δ = 1.82 ppm.

Singlet Oxygen Release Assay. 1,3-Diphenylisobenzofuran (DPBF) was used as the $^1O_2$ scavenger to measure the release of $^1O_2$ at 37 °C or 25 °C.A mixture of DPBF and **Y3** or **Y3-1** was placed in a water bath (37 °C or 25 °C) and covered with foil. The absorption was monitored at 415 nm. The release of $^1O_2$ can be identified as a first-order reaction, according to the first-order reaction kinetic formula: $\ln(A_0/A) = kt$, where A_0 and A are the initial and time-point absorbance values of DPBF, respectively, and k is the DPBF consuming rate, which is the releasing rate of $^1O_2$. The half-life ($t_{1/2}$) value can be calculated by the following formula: $t_{1/2} = \ln2/k$.

Cellular Uptake. HELF, Hcc827, HepG2and H1975 cells were seeded onto a plate and incubated overnight (100 μL, 5000 cells/well). Each cell was set up with six wells. Drugs were

added to the wells (25 μM, 100 μL/well) for 24 h. The plates were gently washed with PBS 3 times. 1% SDS solution (120 μL) was then added to each well to lyse the cells. The fluorescence intensity of drugs (ex/em: 335/481 nm) in the cell extract was measured on a microplate reader. Cellular protein content was determined with a BCA Protien Assay Kit. The cellular uptake is expressed as nmol drug per mg cell protein.

Cellular ROS Assay. Cellular ROS were determined by using a probe DCFH-DA (2',7'-dichlorodihydrofluorescein diacetate) which can form the fluorescent compound DCF (2,7-dichlorofluorescein) in the presence of ROS. The cells were seeded onto a plate and incubated overnight (100 μL, 5000 cells/well). Six replicates per concentration were set for each drug (25 μM, 100 μL/well). A positive control group and a negative control group were used. After 24 h, the plate was washed with PBS, and DCFH-DA (10 μM, 40 μL/well) was added. After 30 min, the plate was washed 3 times with PBS, and 120 μL of 1% SDS lysis buffer was added. The DCF fluorescence was measured by a microplate reader (ex/em: 488/525 nm).

Cytotoxicity Experiment. Hcc827, HepG2 or H1975 cells were seeded onto 96-well plates at 4000 cells per well and incubated overnight. The dissolved drugs (erlotinib, **Y3**, or **Y3-1**) were diluted in culture medium to a series of concentrations. Six replicates per concentration were set for each compound. After 24 h of incubation, 10 μL of MTT solution (5 mg/mL) was added to each well and then the plate was incubated for 4 h. Then, 100 μL of DMSO was added to each well, followed by 20 min incubation. The OD value of each well was measured by a microplate reader (λ_{abs}^{max} = 570 nm).

Flow Cytometric Assay. HepG2 cells were grown to approxiamately 80% confluence and incubated with different concentrations of **Y3-1** for 24 h. Then, the cells were trypsinized and washed three times with PBS. After incubation with the reagents in the Annexin V-FITC/PI

Apoptosis Kit for 20 min in the dark, the cells were analyzed on a BD AccuriTM C6 flow cytometer.

Establishment of H22 Tumor-bearing Mouse Model. Female Kunming mice (4 weeks old, 18-20 g) were purchased from Shanghai SLAC Laboratory Animal Co. Ltd, Shanghai, China. These mice were maintained and handled in accordance with the recommendations of the Institutional Animal Care and Use Committee (IACUC). 200 μL of H22 ascites tumor cell suspension (approximately 5000000 cells/mL) was subcutaneously inoculated into the right side of the mice. *In vivo* imaging and therapy experiments started when the tumor reached 80-100 mm^3 7 days after inoculation.

Fluorescence Molecular Tomography Imaging. H22 tumor-bearing mice were randomly divided into two groups: the erlotinib group (200 μL 0.1 mg/kg erlotinib), and the **Y3-1** group (200 μL 0.1 mg/kg **Y3-1**). Fluorescence molecular tomography imaging was carried out at different time points after the administration.

***In Vivo* Anticancer Assay.** H22 tumor-bearing mice were randomly divided into three groups: the control group (200 μL PBS), erlotinib group (200 μL 0.1 mg/kg erlotinib), and **Y3-1** group (200 μL 0.1 mg/kg **Y3-1**). Tumor growth was monitored by measuring the tumor volume (TV), which is calculated from the length (L) and width (W) of the tumor using the formula ($TV = 0.5 \times L \times W^2$) every day. Body weight was also recorded daily. After 11 days of treatment, the mice were sacrificed and the main organs (heart, liver, spleen, lung, kidney and tumor) were collected and embedded in paraffin and stained with hematoxylin and eosin (H&E).

RESULTS AND DISCUSSION

Design and Synthesis. The synthesis of the title compound **Y3-1** and its related compounds are shown in Scheme 1. Initially, a substitution reaction of alpha,alpha'-dibromo-p-xylene with

sodium azide in N,N-dimethylformamide (DMF) overnight at room temperature yielded a white crystal of **Y1**. Next, **Y2** was obtained through an electrophilic addition reaction of 2-hydroxypyridine with **Y1** using 18-crown-6 and potassium iodide as a catalyst. After irradiation by a 670 nm laser in the presence of methylene blue and oxygen, compound o**Y2** then underwent nucleophilic substitution to give compound **Y2-1**. Subsequently, **Y2-1** performed 1,3-dipolar cycloaddition with erlotinib in the presence of sodium ascorbate and $CuSO_4$ $5H_2O$ to give **Y3-1**. For comparison, **Y2**, which has only a 2-pyridone moiety, also performed 1,3-dipolar cycloaddition with erlotinib to give **Y3** without a $^1O_2$ generation moiety. All these compounds were characterized by ^{1}H NMR, ^{13}C NMR and HRMS (see Supporting Information Figures S1-S12)

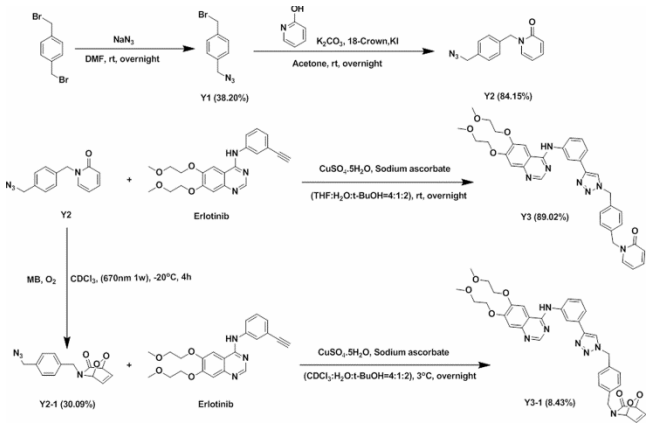

Scheme 1. Synthesis of **Y3-1** and its related compounds.

Singlet Oxygen Release Investigation. The $^1O_2$ release ability of **Y3-1** was first investigated using 1,3-diphenylisobenzofuran (DPBF) as a selective $^1O_2$ quencher at 37 °C or 25 °C in DMF. As shown in Figure 1a, the absorbance of DPBF in **Y3-1** group decreased significantly at 37 °C, while the absorbance values in the control group and **Y3** group did not show obvious changes, indicating that only **Y3-1** can release $^1O_2$ at 37 °C. In addition, the absorbance of DPBF exhibits

a small downtrend at 25 °C in **Y3-1**group (Figure 1b), showing that the $^1O_2$ release ability of **Y3-1** is greatly reduced at 25 °C. These results demonstrated that **Y3-1** can release $^1O_2$ through thermal decomposition. Kinetic stability at body temperature (37 °C) is important. Assuming that the release of $^1O_2$ follows a first-order reaction kinetics mode, the $\ln(A_0/A)$ vs. time is shown in Figure 1c. According to the half-life formula of the drugs, $t_{1/2} = 0.693/k$, the half-life of **Y3-1** can be calculated to be 13.0 h.

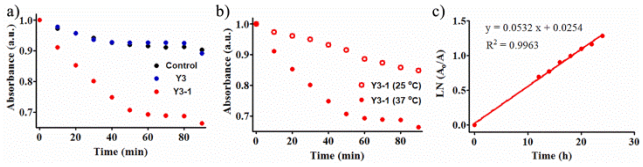

Figure 1. a) Decrease in the absorbance of DPBF at 415 nm with time in the presence of no drug (control group), **Y3** or **Y3-1** in DMF at 37 °C. b) Decrease in the absorbance of DPBF at 415 nm with time in the presence of **Y3-1** in DMF at 37 °C and 25 °C. c) Plot of $Ln(A_0/A)$ of **Y3-1** vs. time, A0 is the absorbance value of DPBF at 0 h. The concentration of **Y3** or **Y3-1** is 1.47 mM.

***In Vitro* Cancer Targeting.** To demonstrate the cancer targeting ability of the erlotinib moiety in **Y3-1**, three cancer cells: Hcc827 cells (erlotinib-sensitive human non-small cell lung cancer cells with high EGFR expression), HepG2 cells (Cancer cells with high differentiation and proliferation) and H1975 cells (erlotinib-resistant human non-small cell lung adenocarcinoma cells) were selected. The cellular uptake of **Y3-1** in these three cancer cells was examined by measuring the fluorescence emission intensity of **Y3-1** and the cell protein concentration in the cell extract. The average relative cellular uptake (nmol/mg protein) data are shown in Figure 2. The cellular uptake of **Y3-1** in Hcc827 cells was very significantly higher than that in H1975 cells ($p < 0.001$), and significantly higher than that in HepG2 cells ($p < 0.01$). The differences in the cellular uptake of **Y3-1** are consistent with the erlotinib sensitivity of these cancer cells. The

results demonstrate that the presence of the erlotinib moiety in **Y3-1** results in targeted delivery to cancer cells with higher sensitivity to erlotinib.

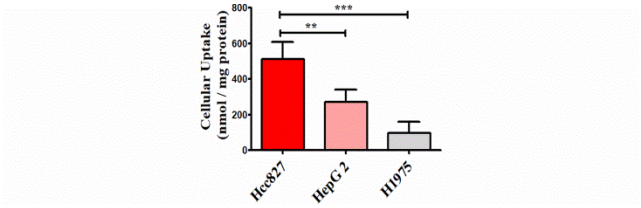

Figure 2. The cellular uptake of **Y3-1** in different cancer cells with different erlotinib sensitivities (six replicates for each group, ** indicates $p < 0.01$, *** indicates $p < 0.001$).

***In Vitro* Anticancer Assay.** The cellular generation efficiency of $^1O_2$ is a critical parameter for the anticancer effect of **Y3-1**. Therefore, the ROS probe DCFH-DA (2',7'-dichlorodihydrofluorescein diacetate) was used to detect intracellular ROS, including $^1O_2$ in Hcc827 cells after 25 μM drug treatment. Compared with the two control drugs **Y3** and erlotinib, our targeted drug **Y3-1** could release significantly more $^1O_2$ in Hcc827 cells (Figure 3a). There was no significant difference in ROS production efficiency between erlotinib and **Y3**, which contains no endoperoxide moiety to store and release $^1O_2$. In addition, the ROS production efficiency of **Y3-1** positively correlated with the concentrations of **Y3-1** in Hcc827 cells (Figure S13, Supporting Information). Therefore, all these results indicate that the combination of reversible singlet-oxygen storage modules and erlotinib can deliver and release $^1O_2$ into cancer cells.

The anticancer effects of **Y3-1**, **Y3** and erlotinib were studied by MTT assays in Hcc827 cells, HepG2 cells and H1975 cells. The dose-dependent survival curves and corresponding IC_{50} values are shown in Figure 2b and Table S1 (Supporting Information). No significant difference was observed in the cellular antiproliferative ability of **Y3** (with IC_{50} = 37.99-68.82 μM) and

erlotinib (with IC_{50} = 33.68-76.67 μM) towards these tree cancer cell lines, indicating that the introduction of the pyridone moiety to the erlotinib unit does not obviously influence its anticancer effects. As expected, **Y3-1**, **Y3-1** armed with $^1O_2$, showed approximately 2-fold higher cytotoxicity (IC_{50} values of 13.52-38.16 μM) than **Y3** or erlotinib, even in erlotinib-resistant cancer cells. The anticancer effect of **Y3-1** in different tumor cells is consistent with its cellular uptake in different cells, which is related to the erlotinib differences in these cancer cells. In addition, the flow cytometric assay of Annexin V-FITC/PI was utilized to further validate the mode of cell death caused by **Y3-1**. As shown in Figure 3c and Figure S14 (Supporting Information), the populations of apoptotic cells (upper right and low right phases) and necrotic cells (upper left phase) increased significantly with increasing **Y3-1** concentration. These results clearly show that **Y3-1** can induce apoptosis and necrosis in tumor cells by mimicking the $^1O_2$-dependent anticancer mechanismof PDT in the absence of light and oxygen.

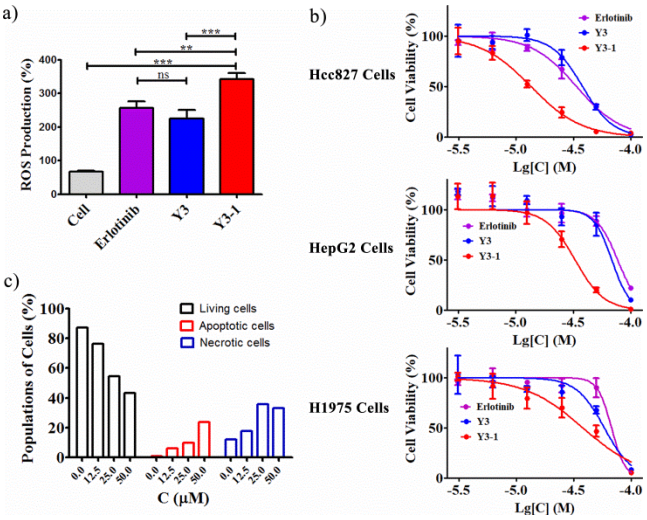

Figure 3. a) Cellular ROS generation in Hcc827 cells by erlotinib, **Y3** and **Y3-1** (the drug concentration is 25 μM, six replicates are used for each group, ** indicates $p < 0.01$, *** indicates $p < 0.001$, ns indicates $p > 0.05$). b) Cytotoxic effects of erlotinib, **Y3**, and **Y3-1** towards Hcc827 cells, HepG2 cells or H1975 cells (data are expressed as the means ± SD from

three experiments, each performed in quadruplicate). c) Histogram of cell populations after 0.0, 12.5 and 50 μM **Y3-1** treatment by Annexin V-FITC/PI detection.

***In Vivo* Cancer Targeting.** To further confirm the precise delivery of **Y3-1** to the tumor by the erlotinib moiety, *in vivo* fluorescence imaging was also performed by using the FMT (fluorescence molecular tomography) TM 2500 system (PerkinElmer Inc.). For this purpose, 0.1 mg/kg **Y3-1** (labeled with Cy5 NHS ester) or erlotinib (labeled with Cy5 Azide) was injected into the tail vein of Kunming mice bearing H22 tumors. As shown in Figure 4a-b, **Y3-1** exhibited an increasing accumulation in tumor tissue within 8 h and then gradually decreased. The highest accumulation time was much shorter than the half-life of **Y3-1**, enabling **Y3-1** release $^1O_2$ and achieve excellent anticancer effects. Skin phototoxicity, which results from drug accumulation in skin tissue, is still a fundamental barrier to the clinical application of PDT. Therefore, we also studies **Y3-1** accumulation in normal skin tissues. As shown in Figure 4a-b, no visible accumulation appeared in normal skin tissues over time. Additionally, the total amount of **Y3-1** or erlotinib in the tumor tissue was obviously higher than that in normal skin tissue (Figure 4). This result indicates the high specificity of **Y3-1** to tumors, which can be attributed to the erlotinib moiety with its high targeting ability towards tumor tissues.

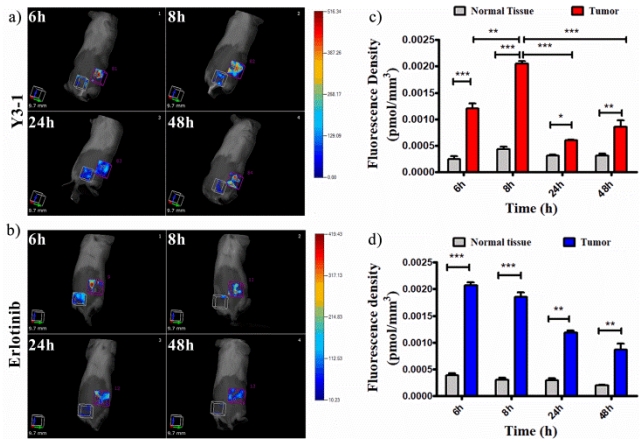

Figure 4. *In vivo* cancer targeting investigation by using Kunming mice bearing subcutaneous H22 tumors. 3D fluorescence images based on FMT after administration with (a) **Y3-1** or (b) erlotinib. Comparison of the average fluorescence density of drugs in normal skin tissue and tumor after administration with (c) **Y3-1** or (d) erlotinib (** indicates $p < 0.01$, *** indicates $p < 0.001$).

***In Vivo* Anticancer Assay.** To further investigate the *in vivo* anticancer effect of **Y3-1**, H22 tumors were established in Kunming mice. When the tumor volume reached 50-80 mm^3, 0.1 mg/kg **Y3-1** or erlotinib was injected into the mouse tail vein in the test group, while the control group was treated with PBS. As shown in Figure 5a and c, erlotinib could partially decrease tumor volume compared with that in the control group. Moreover, we found that **Y3-1** induced a complete tumor inhibition with a significant difference ($p < 0.01$) compared with erlotinib group and an extremely significant difference ($p < 0.001$) compared with the control group. We also examined hematoxylin-eosin (H&E) staining on tumor sections (Figure 5d). Compared with the control group and erlotinib group, **Y3-1** group contained more deformed nuclei (karyopyknosis, karyorrhexis, and karyolysis), which indicates severe necrosis of cancer cells. The enhanced in vivo anticancer effect of **Y3-1** may be attributed to its singlet oxygen chemical source endoperoxide acting like PDT-based mechanisms supported by accumulating evidence: directly killing cancer cells, shutting down the tumor microvasculature and inducing antitumor immunity. These data provide support for the excellent anticancer performance of **Y3-1** through the EGFR-targeted delivery of the thermal-controlled release singlet oxygen sensitizer inspired by targeted PDT-based mechanisms.

To study the biosafety of **Y3-1**, we examined the body weight and the HE staining of other normal organs. As shown in Figure 5b and d, no loss of body weight or other signs of toxicity

manifested following the drugs administration (Figure 5b) and no obvious pathological alterations were observed in the HE staining of the heart, liver, spleen, lung and kidney in all mice after 11 days of treatment (Figure 5d). These results indicate that **Y3-1** has a high biosafety index.

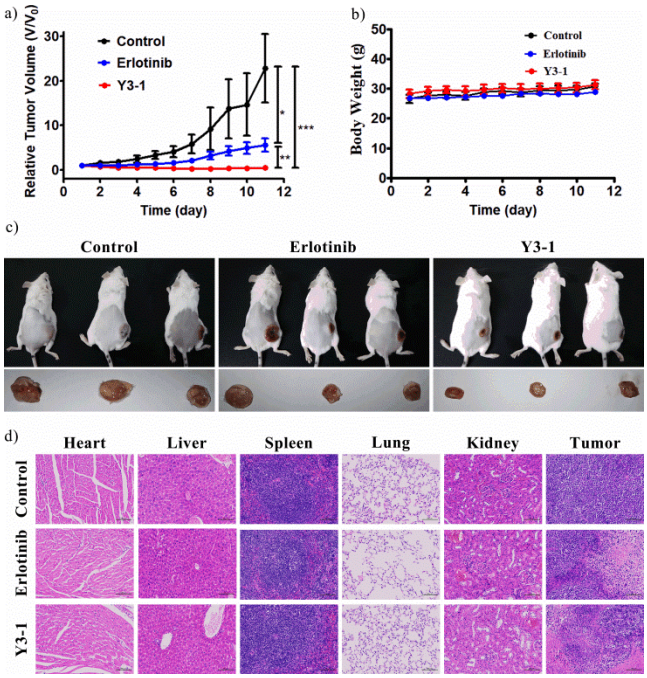

Figure 5. a) Tumor volume curves of mice treated with solvent, erlotinib and **Y3-1**. b) Body weight curves of mice treated with solvent, erlotinib and **Y3-1**. c) Photos of mice and excise tumors after treatment on the 11th day. d) HE staining of tumor sections and major organs (heart, liver, spleen, lung and kidney) from H22 tumor bearing mice on the 11th day. The scale bars are 100 μm.

In conclusion, we successfully developed a proof of principle concept for targeted anticancer therapy by introducing an EGFR targeting moiety into a PDT-mimetic sensitizer, which does not require *in vivo* oxygen or light. We demonstrated that singlet oxygen, the key factor in PDT, can be stored in **Y3-1** by *in vitro* photosensitization and be precisely delivered into EGFR-

overexpressing cancer cells/tissues. Additionally, our results clearly confirmed the excellent anticancer efficacy of **Y3-1** achieved by the delivery of thermal-release singlet oxygen. As the first demonstration, this smart strategy might provide a new concept and model for the further development of more efficient anticancer drugs. Other drugs based on this strategy are currently ongoing in our lab and further results will be reported soon.

ASSOCIATED CONTENT

Supporting Information

The Supporting Information is available free of charge on the ACS Publications website at DOI: Cellular antiproliferative activities, ROS production, Flow apoptotic results, ^{1}H NMR, ^{13}C NMR and HRMS spectra characterization (PDF)

AUTHOR INFORMATION

Corresponding Author

*E-mail: xuejinping66@fzu.edu.cn. Phone: +86-0591-2286-7923. Fax: +86-0591-2286-7923.

ORCID

Juanjuan Chen: 0000-0002-9148-2206

Jinping Xue: 0000-0001-6952-0475

Author Contributions

$^{\perp}$J. C. and D. L. contributed equally to this work.

Notes

The authors declare no competing financial interest.

ACKNOWLEDGMENT

This work was supported by the National Natural Science Foundation of China (81703345, 81803346, 51672046), and the National Health and Family Planning Commission jointly established a scientific research fund (WKJ2016-2-14).

ABBREVIATIONS

PDT, photodynamic therapy; EGFR, epidermal growth factor; PSs, photosensitizers; DMF, N,N dimethylformamide; DPBF, 1,3-diphenylisobenzofuran; ROS, reactive oxygen species; DCFH-DA, 2',7'-dichlorodihydrofluorescein diacetate; H&E, hematoxylin-eosin.

REFERENCES

(1) Dolmans, D. E. J. G. J.; Fukumura, D.; Jain, R. K. Photodynamic therapy for cancer. *Nat. Rev. Cancer* **2003**, *3*, 380-387.

(2) Castano, A. P.; Mroz, P.; Hamblin, M. R. Photodynamic therapy and anti-tumour immunity. *Nat. Rev. Cancer* **2006**, *6*, 535-545.

(3) Majumdar, P.; Nomula, R.; Zhao, J. Activatable triplet photosensitizers: Magic bullets for targeted photodynamic therapy. *J. Mater. Chem.* C **2014**, *2*, 5982-5997.

(4) Shen, Y.; Shuhendler, A. J.; Ye, D.; Xu, J.-J.; Chen, H.-Y. Two-photon excitation nanoparticles for photodynamic therapy. *Chem. Soc. Rev.* **2016**, *45*, 6725-6741.

(5) Celli, J. P.; Spring, B. Q.; Rizvi, I.; Evans, C. L.; Samkoe, K. S.; Verma, S.; Pogue, B. W.; Hasan, T. Imaging and photodynamic therapy: Mechanisms, monitoring, and optimization. *Chem. Rev.* **2010**, *110*, 2795-2838.

(6) Kamkaew, A.; Lim, S.H.; Lee, H.B.; Kiew, L.V.; Chung, L.Y.; Burgess, K. BODIPY dyes in photodynamic therapy. *Chem. Soc. Rev.* **2013**, *42*, 77-88.

(7) Zhou, Z.; Song, J.; Nie, L.; Chen, X. Reactive oxygen species generating systems meeting challenges of photodynamic cancer therapy. *Chem. Soc. Rev.* **2016**, *45*, 6597-6626.

(8) Stolik, S.; Delgado, J. A.; Perez, A.; Anasagasti, L. Measurement of the penetration depths of red and near infrared light in human "Ex vivo" Tissues. *J. Photochem. Photobiol. B-Biol.* **2000**, *57*, 90-93.

(9) Ethirajan, M.; Chen, Y.; Joshi, P.; Pandey, R. K. The role of porphyrin chemistry in tumor imaging and photodynamic therapy. *Chem. Soc. Rev.* **2011**, *40*, 340-362.

(10) Idris, N. M.; Gnanasammandhan, M. K.; Zhang, J.; Ho, P. C.; Mahendran, R.; Zhang, Y. In vivo photodynamic therapy using upconversion nanoparticles as remote-controlled nanotransducers. *Nat. Med.* **2012**, *18*, 1580-1585.

(11) Roberts, W. G.; Smith, K. M.; Mcculiough, J. L.; Berns, M. W. Skin photosensitivity and photodestruction of several potential photodynamic sensitizers. *Photochem. Photobiol.* **1989**, *49*, 431-438.

(12) Dong, Z.; Feng, L.; Hao, Y.; Chen, M.; Gao, M.; Chao, Y.; Zhao, H.; Zhu, W.; Liu, J.; Liang, C.; Zhang, Q.; Liu, Z. Synthesis of hollow biomineralized caco3–polydopamine nanoparticles for multimodal imaging-guided cancer photodynamic therapy with reduced skin photosensitivity. *J. Am. Chem. Soc.* **2018**, *140*, 2165-2178.

(13) Sitnik, T. M.; Hampton, J. A.; Henderson, B. W. Reduction of tumour oxygenation during and after photodynamic therapy in vivo: Effects of fluence rate. *Brit. J. Cancer* **1998**, *77*, 1386-1394.

(14) Busch, T. M.; Hahn, S. M.; Evans, S. M.; Koch, C. J. Depletion of tumor oxygenation during photodynamic therapy: Detection by the hypoxia marker EF3 [2-(2-nitroimidazol-1[h]-yl)-n-(3,3,3-trifluoropropyl)acetamide]. *Cancer Res.* **2000**, *60*, 2636-2642.

(15) Sullivan, R.; Graham, C. H. Hypoxia-driven selection of the metastatic phenotype. *Cancer Metast. Rev.* **2007**, *26*, 319-331.

(16) H Sibata, C.; Colussi, V.; Oleinick, N.; Kinsella, T. Photodynamic therapy in oncology. *Expert. Opin. Pharmacother*. **2001**, *2*, 917-927.

(17) Monro, S.; Colón, K.L.; Yin, H.; Roque, J.; Konda, P.; Gujar, S.; Thummel, R.P.; Lilge, L.; Cameron, C.G.; McFarland, S.A. Transition metal complexes and photodynamic therapy from a tumor-centered approach: Challenges, opportunities, and highlights from the development of tld1433. *Chem. Rev.* **2019**, *119*, 797-828.

(18) Baumes, J. M.; Gassensmith, J. J.; Giblin, J.; Lee, J.-J.; White, A. G.; Culligan, W. J.; Leevy, W. M.; Kuno, M.; Smith, B. D. Storable, thermally activated, near-infrared chemiluminescent dyes and dye-stained microparticles for optical imaging. *Nat. Chem.* **2010**, *2*, 1025-1030.

(19) Wiegand, C.; Herdtweck, E.; Bach, T. Enantioselectivity in visible light-induced, singlet oxygen [2+4] cycloaddition reactions (type ii photooxygenations) of 2-pyridones. *Chem. Commun.* **2012**, *48*, 10195-10197.

(20) Posavec, D.; Zabel, M.; Bogner, U.; Bernhardt, G.; Knor, G. Functionalized derivatives of 1,4-dimethylnaphthalene as precursors for biomedical applications: Synthesis, structures, spectroscopy and photochemical activation in the presence of dioxygen. *Org. Biomol. Chem.* **2012**, *10*, 7062-7069.

(21) Benz, S.; Notzli, S.; Siegel, J. S.; Eberli, D.; Jessen, H. J. Controlled oxygen release from pyridone endoperoxides promotes cell survival under anoxic conditions. *J. Med. Chem.* **2013**, *56*, 10171-10182.

(22) Turan, I. S.; Yildiz, D.; Turksoy, A.; Gunaydin, G.; Akkaya, E. U. A bifunctional photosensitizer for enhanced fractional photodynamic therapy: Singlet oxygen generation in the presence and absence of light. *Angew. Chem. Int. Edit.* **2016**, *55*, 2875-2878.

(23) Changtong, C.; Carney, D. W.; Luo, L.; Zoto, C. A.; Lombardi, J. L.; Connors, R. E. A porphyrin molecule that generates, traps, stores, and releases singlet oxygen. *J. Photochem. Photobiol. A* **2013**, *260*, 9-13.

(24) Filatov, M. A.; Heinrich, E.; Busko, D.; Ilieva, I. Z.; Landfester, K.; Baluschev, S. Reversible oxygen addition on a triplet sensitizer molecule: Protection from excited state depopulation. *Phys. Chem. Chem. Phys.* **2015**, *17*, 6501-6510.

(25) Callaghan, S.; Filatov, M. A.; Sitte, E.; Savoie, H.; Senge, M. O. Delayed release singlet oxygen sensitizers based on pyridone-appended porphyrins. *Photochem. Photobiol. Sci.* **2017**, *16*, 1371-1374.

(26) Kolemen, S.; Ozdemir, T.; Lee, D.; Kim, G. M.; Karatas, T.; Yoon, J.; Akkaya, E. U. Remote-controlled release of singlet oxygen by the plasmonic heating of endoperoxide-modified gold nanorods: Towards a paradigm change in photodynamic therapy. *Angew. Chem. Int. Edit.* **2016**, *55*, 3606-3610.

(27) Pollack, V. A.; Savage, D. M.; Baker, D. A.; Tsaparikos, K. E.; Sloan, D. E.; Moyer, J. D.; Barbacci, E. G.; Pustilnik, L. R.; Smolarek, T. A.; Davis, J. A. Inhibition of epidermal growth factor receptor-associated tyrosine phosphorylation in human carcinomas with cp-358,774: Dynamics of receptor inhibition in situ and antitumor effects in athymic mice. *J. Pharmacol. Exp. Ther.* **1999**, *291*, 739-748.

(28) Johnson, J. R.; Cohen, M.; Sridhara, R.; Chen, Y.-F.; Williams, G. M.; Duan, J.; Gobburu, J.; Booth, B.; Benson, K.; Leighton, J.; Hsieh, L. S.; Chidambaram, N.; Zimmerman, P.; Pazdur,

R. Approval summary for erlotinib for treatment of patients with locally advanced or metastatic non–small cell lung cancer after failure of at least one prior chemotherapy regimen. *Clin. Cancer Res.* **2005**, *11*, 6414-6421.

(29) Carey, K. D.; Garton A. J.; Romero, M. S.; Kahler, J.; Thomson, S.; Ross, S.; Park, F.; Haley, J. D.; Gibson, N.; Sliwkowski, M. X. Kinetic analysis of epidermal growth factor receptor somatic mutant proteins shows increased sensitivity to the epidermal growth factor receptor tyrosine kinase inhibitor, erlotinib. *Cancer Res.* **2006**, *66*, 8163-8171.

(30) Cataldo, V. D.; Gibbons, D. L.; Pérez-Soler, R.; Quintás-Cardama, A. Treatment of non–small-cell lung cancer with erlotinib or gefitinib. *New Engl. J. Med.* **2011**, *364*, 947-955.

(31) Zhang, F.-L.; Huang, Q.; Zheng, K.; Li, J.; Liu, J.-Y.; Xue, J.-P. A novel strategy for targeting photodynamic therapy. Molecular combo of photodynamic agent zinc(ii) phthalocyanine and small molecule target-based anticancer drug erlotinib. *Chem. Commun.* **2013**, *49*, 9570-9572.

(32) Zhang, F.-L.; Huang, Q.; Liu, J.-Y.; Huang, M.-D.; Xue, J.-P. Molecular-target-based anticancer photosensitizer: Synthesis and in vitro photodynamic activity of erlotinib–zinc(ii) phthalocyanine conjugates. *ChemMedChem* **2015**, *10*, 312-320.

(33) Chen, J.; Ye, H.; Zhang, M.; Li, J.; Liu, J.; Xue, J. Erlotinib analogue-substituted zinc(ii) phthalocyanines for small molecular target-based photodynamic cancer therapy. *Chin. J. Chem.* **2016**, *34*, 983-988.

(34) Nian, F.; Huang, Y.; Song, M.R.; Chen, J.J.; Xue, J. A novel fabricated material with divergent chemical handles based on uio-66 and used for targeted photodynamic therapy. *J. Mater. Chem. B* **2017**, *5*, 6227-6232.

(35) Chen, J.-J.; Huang, Y.-Z.; Song, M.-R.; Zhang, Z.-H.; Xue, J.-P. Silicon phthalocyanines axially disubstituted with erlotinib toward small-molecular-target-based photodynamic therapy. *ChemMedChem* **2017**, *12*, 1504-1511.

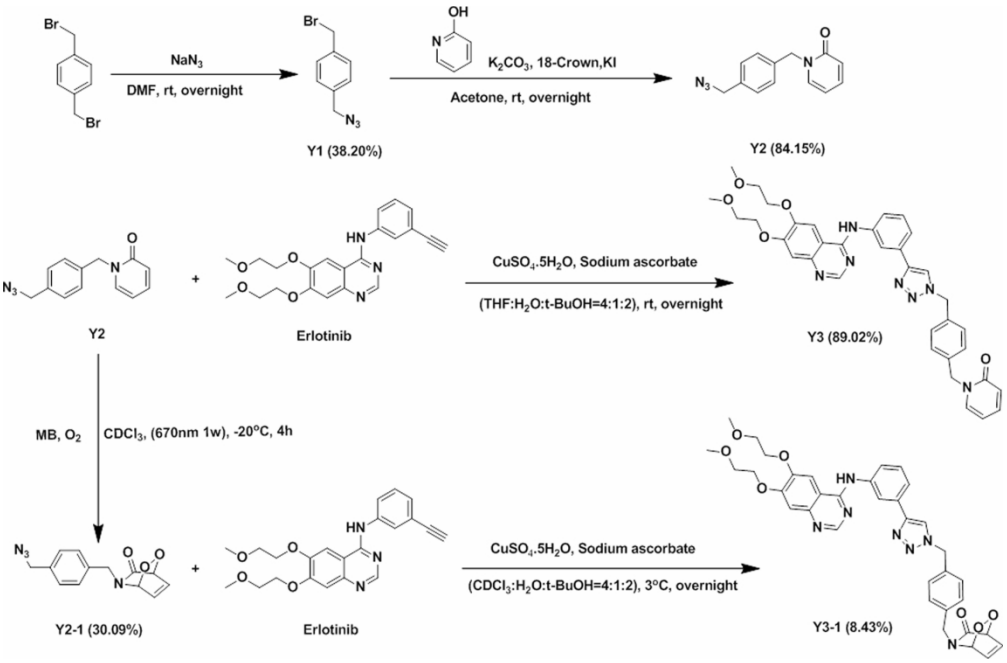

Scheme 1. Synthesis of **Y3-1** and its related compounds.

84x55mm (600 x 600 DPI)

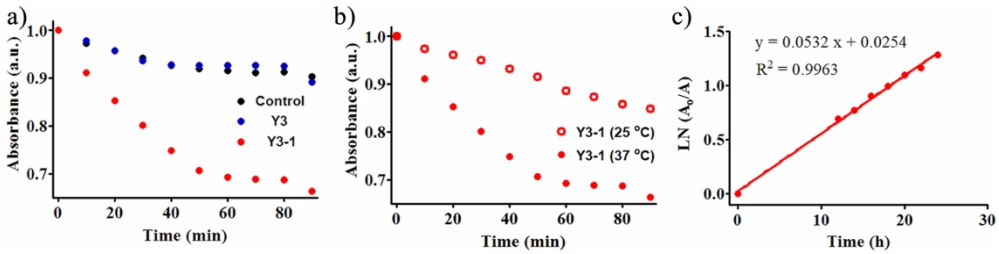

Figure 1. a) Decrease in the absorbance of DPBF at 415 nm with time in the presence of no drug (control group), **Y3** or **Y3-1** in DMF at 37 °C. b) Decrease in the absorbance of DPBF at 415 nm with time in the presence of **Y3-1** in DMF at 37 °C and 25 °C. c) Plot of $Ln(A_0/A)$ of **Y3-1** vs. time, A0 is the absorbance value of DPBF at 0 h. The concentration of **Y3** or **Y3-1** is 1.47 mM.

84x21mm (600 x 600 DPI)

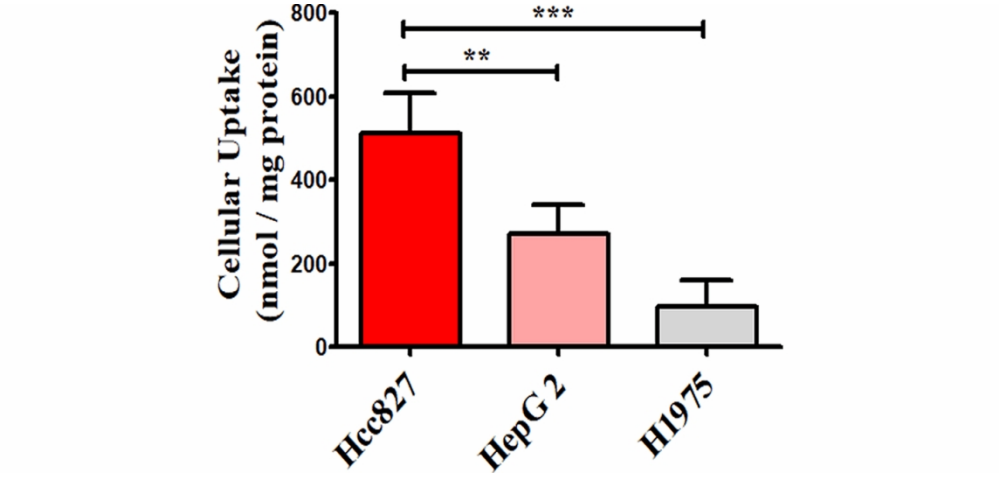

Figure 2. The cellular uptake of **Y3-1** in different cancer cells with different erlotinib sensitivities (six replicates for each group, ** indicates $p < 0.01$, *** indicates $p < 0.001$).

84x39mm (600 x 600 DPI)

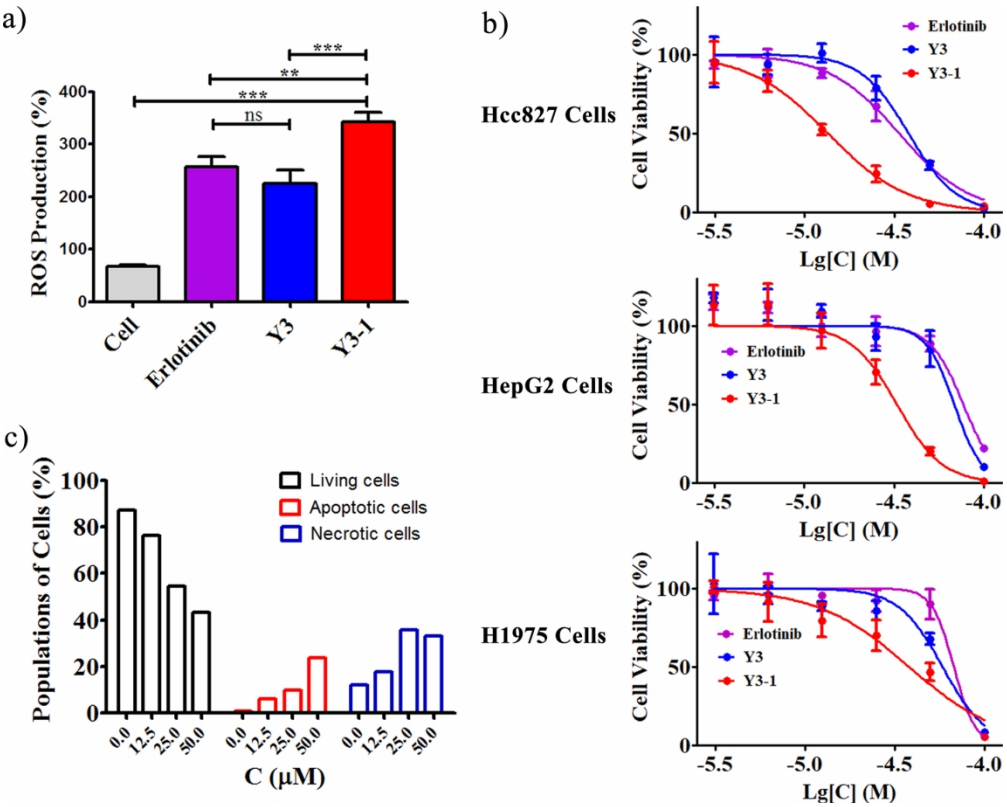

a) Cellular ROS generation in Hcc827 cells by erlotinib, **Y3** and **Y3-1** (the drug concentration is 25 μM, six replicates are used for each group, ** indicates $p < 0.01$, *** indicates $p < 0.001$, ns indicates $p > 0.05$). b) Cytotoxic effects of erlotinib, **Y3**, and **Y3-1** towards Hcc827 cells, HepG2 cells or H1975 cells (data are expressed as the means ± SD from three experiments, each performed in quadruplicate). c) Histogram of cell populations after 0.0, 12.5 and 50 μM **Y3-1** treatment by Annexin V-FITC/PI detection.

84x67mm (600 x 600 DPI)

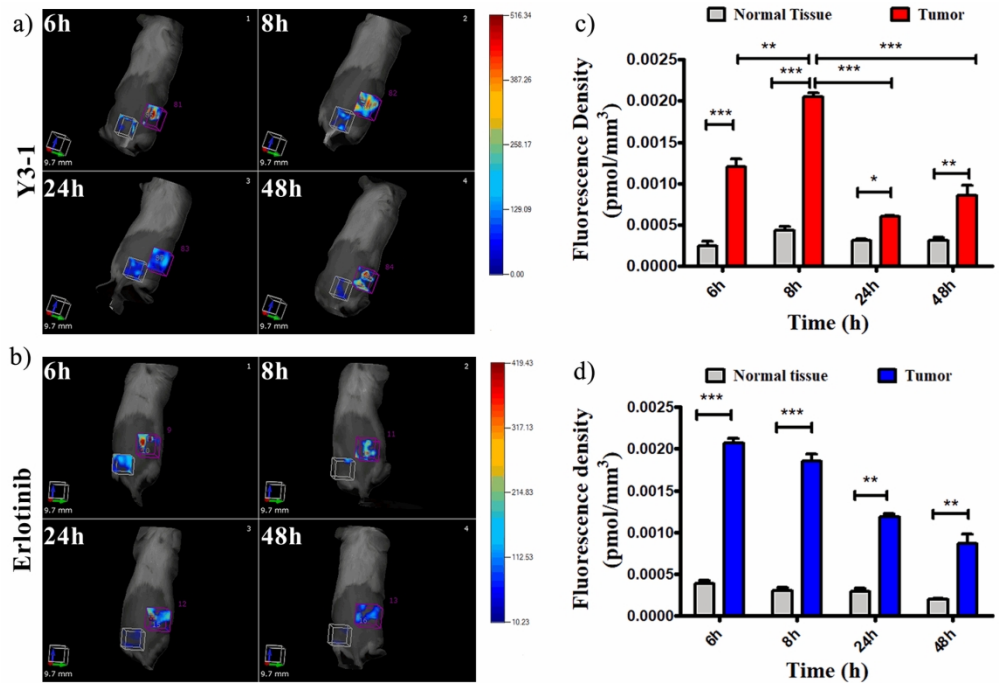

In vivo cancer targeting investigation by using Kunming mice bearing subcutaneous H22 tumors. 3D fluorescence images based on FMT after administration with (a) **Y3-1** or (b) erlotinib. Comparison of the average fluorescence density of drugs in normal skin tissue and tumor after administration with (c) **Y3-1** or (d) erlotinib (** indicates $p < 0.01$, *** indicates $p < 0.001$).

84x57mm (600 x 600 DPI)

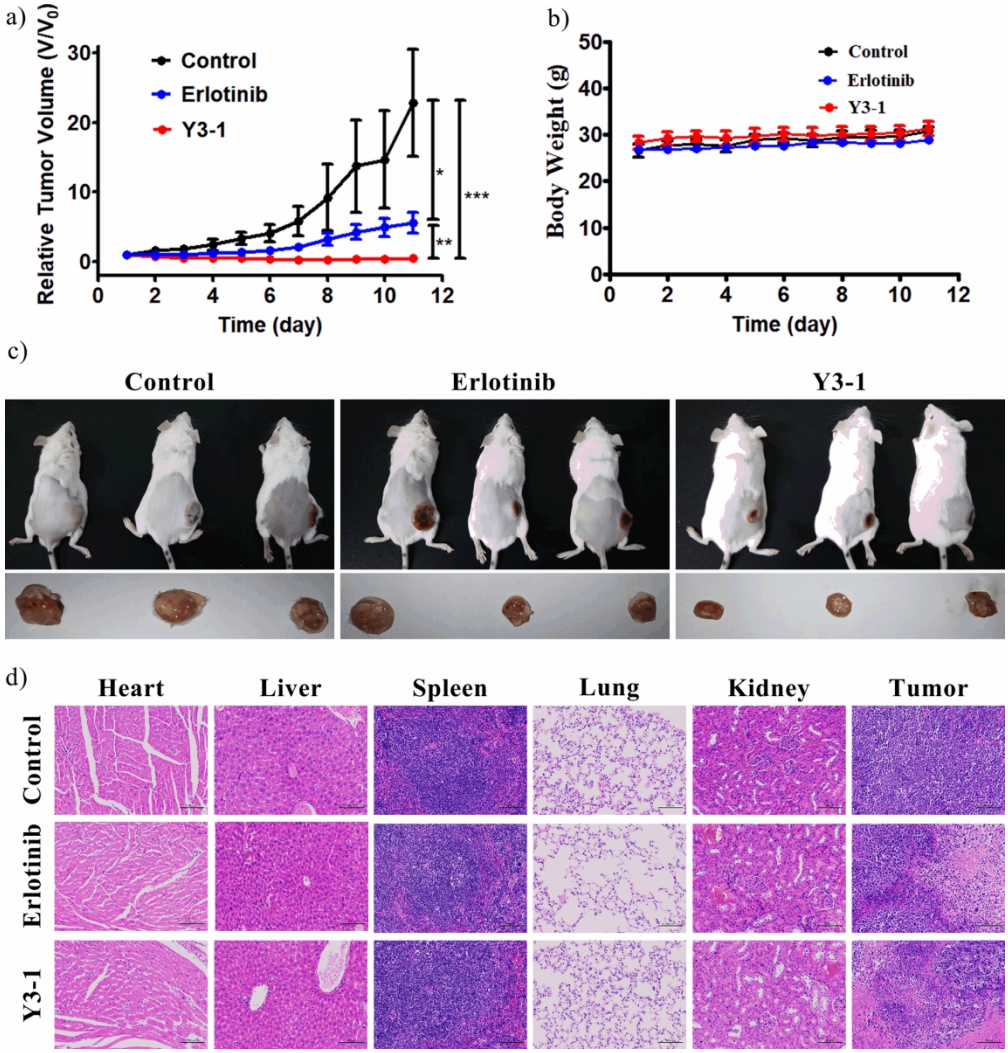

a) Tumor volume curves of mice treated with solvent, erlotinib and **Y3-1**. b) Body weight curves of mice treated with solvent, erlotinib and **Y3-1**. c) Photos of mice and excise tumors after treatment on the 11th day. d) HE staining of tumor sections and major organs (heart, liver, spleen, lung and kidney) from H22 tumor bearing mice on the 11th day. The scale bars are 100 μm.

84x88mm (600 x 600 DPI)